THE JOURNAL OF PHYSICAL CHEMISTRY C

Article

pubs.acs.org/JPCC

Interconversion of α-Fe_2O_3 and Fe_3O_4 Thin Films: Mechanisms, Morphology, and Evidence for Unexpected Substrate Participation

Francesca Genuzio, Alessandro Sala, Thomas Schmidt,* Dietrich Menzel, and Hans-Joachim Freund

Department of Chemical Physics, Fritz Haber Institute of the Max Planck Society, Faradayweg 4-6, 14195 Berlin, Germany

ABSTRACT: The reversible transformations of thin magnetite (Fe_3O_4) and hematite (α-Fe_2O_3) films grown on Pt(111) and Ag(111) single crystals as support have been investigated by a combined low energy electron microscopy (LEEM) and low-energy electron diffraction (LEED) study. The conversions were driven by oxidation, annealing in ultrahigh vacuum (UHV), or Fe deposition with subsequent annealing. As expected, the oxidation of a Fe_3O_4 film yielded an α-Fe_2O_3 structure. Unexpectedly, the annealing in UHV also led to a transformation from Fe_3O_4 into α-Fe_2O_3, but only if Pt(111) was used as substrate. In contrast, on a Ag(111) substrate the inverse reaction, a slow transformation from α-Fe_2O_3 into Fe_3O_4, was observed, as expected for oxygen desorption. Fe deposition on α-Fe_2O_3 and subsequent annealing in UHV transformed the film into Fe_3O_4. As the most probable explanation we propose that the UHV conversion on Pt(111) supports proceeds by Fe cation diffusion through the film and Fe atom dissolution in the substrate, decreasing the Fe concentration within the iron oxide film. This process is not possible for a Ag(111) substrate. The interconversions, which were best observable in mixed films containing domains of both oxides, occurred by growth of one domain type with well-defined boundaries and growth rates.

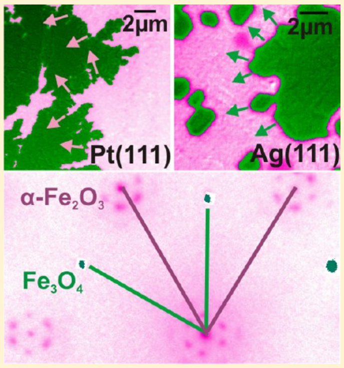

1. INTRODUCTION

The investigation of iron oxide films and their surfaces has developed into a promising research field, due to their many technological applications, ranging from magnetic devices to heterogeneous catalysis.[1,2] This class of material exhibits rather different magnetic or conducting properties[3,4] depending on their crystal structures, which is strongly determined by the way of preparation.

During recent years, increasing numbers of studies have addressed the issue of growth conditions of well-defined oxide film systems, indicating that the film stability depends on many parameters, which may differ significantly from those predicted via a bulk oxide phase diagram.[5−9] In the case of thin oxide films, the influence of the supporting metal substrate has to be taken into account, also. Karunamuni et al. suggested[10] that in general distinct phase diagrams have to be considered for each kind of substrate. Unfortunately, only very few systematic studies have addressed these issues.

Magnetite (Fe_3O_4) and hematite (α-Fe_2O_3) are the most frequently investigated iron oxides since they are the most stable and common phases existing in nature, but there are also metastable phases known, such as γ-Fe_2O_3, ε-Fe_2O_3, etc.[1] In particular, Fe_3O_4 and α-Fe_2O_3 thin films have been successfully grown on many substrates,[11−14] by Fe deposition and oxidation in a wide temperature and pressure range.[15] Even though it has been known since the 1990s that different surface terminations are formed depending on preparation conditions,[16] no unambiguous model exists up to now which explains this variability coherently.[17]

The reversible transformation between α-Fe_2O_3 and Fe_3O_4 has been investigated by different groups using low-energy electron diffraction (LEED),[13,18,19] surface X-ray diffraction (SXRD),[13] scanning tunneling microscopy (STM),[19] and low energy electron microscopy (LEEM)[18] using either iron oxide single crystals or thin films grown on different substrates, with special focus on the stability of the different phases. The oxidation of Fe_3O_4 leads to γ-(maghemite) and α-Fe_2O_3 (hematite) allotropes; the reasons for the different structural results have been debated in the literature already in the 1960s[20−23] with the conclusion that the temperature required to enable the structural transformation of Fe_3O_4 to α-Fe_2O_3 is influenced by crystal size and impurities already present in the samples. Therefore, studying well-defined systems and understanding their stability conditions are fundamental. Moreover, controlling the preparation parameters is essential for the growth of thin oxide films on single-crystal surfaces, as they are used as model systems (e.g., for heterogeneous catalysis).[24]

For a transformation between the two crystalline phases of Fe_3O_4 and α-Fe_2O_3, both the crystal structure and the stoichiometry have to change. In principle, at least four possible types of reactions can change the stoichiometry of the two iron phases. The two processes, yielding Fe_2O_3 (oxidation and redox-reaction, respectively) are

$$4Fe_3O_4 + O_2 \rightarrow 6Fe_2O_3$$

$$3Fe_3O_4 \rightarrow 4Fe_2O_3 + Fe$$

and the inverse processes (reduction) are

Special Issue: John C. Hemminger Festschrift

Received: April 24, 2014
Revised: September 12, 2014
Published: September 16, 2014

$$6Fe_2O_3 \rightarrow 4Fe_3O_4 + O_2$$

$$4Fe_2O_3 + Fe \rightarrow 3Fe_3O_4$$

In this paper, we present a combined LEEM and LEED study to characterize systematically the conditions for reverse transformations between these two oxide phases. Some supporting X-ray photoelectron spectroscopy (XPS) and X-ray photoemission electron microscopy (XPEEM) results are also described. The iron oxide films were grown as about 10 nm thin films on two different single-crystal substrates, Pt(111) and Ag(111), in order to study substrate effects. In this work, we found conditions under which Fe_3O_4 is reversibly converted into α-Fe_2O_3 on both substrates, however with different driving forces for the transformation.

2. EXPERIMENTAL PROCEDURES AND SAMPLE PREPARATION

Experiments were carried out in the SMART spectromicroscope, an aberration-corrected and energy-filtered LEEM–PEEM system which combines spectroscopy (XPS, NEXAFS), microscopy (LEEM, PEEM, XPEEM), and diffraction techniques (LEED, SPA-LEED) for a comprehensive characterization of the sample surface. The high acquisition rate allows the observation of processes like growth, chemical reaction, and phase transitions on the surface in *real time* (with time scales of typically one image per second) and *in situ*.[25−27]

Iron oxide thin films were grown on clean Pt(111) and Ag(111) single-crystal substrates by repeated cycles of iron deposition and oxidation at elevated temperature.[6,15] The *in situ* preparation in the main chamber of the SMART microscope allows us to directly follow the processes and to check the quality of the growing film.[9] The Pt(111) and Ag(111) surfaces were cleaned by repeated cycles of argon sputtering and UHV annealing at 1100 and 830 K, respectively, until a sharp LEED pattern without a structured background was obtained. A final oxygen treatment at 1×10^{-6} mbar and 700 K, followed by annealing in ultrahigh vacuum (UHV), removed carbon contaminations, as checked with XPS.

The specimen chamber of SMART with a base pressure of 1×10^{-10} mbar is suited for operation in an oxygen pressure ranging up to 10^{-5} mbar. The single crystals were mounted on a commercial and transferable ELMITEC sample holder with a Mo cap fixing the sample, which was heated from the back side either by radiation from a filament for $T < 700$ K or by electron bombardment for $T > 700$ K with maximum of 2000 K. The temperature was measured with an absolute accuracy of about 10 K by a W26%Re/W5%Re thermocouple, spot-welded to the crystal support. Oxygen (99.999% purity) was dosed by a leak valve directly into the main chamber of the microscope; iron (99.995% purity, Alfa Aesar) was vapor deposited using a commercial evaporator (Omicron EFM3 with ion suppressor) pointing toward the sample under grazing incidence of 20°.

In LEEM the collimated electron beam of a field emitter gun illuminates the sample surface, and the reflected electrons are imaged by a magnifying lens system on a 2D detector, where a CCD camera records the images in about video rate. Secondary and inelastically backscattered electrons are cut off by the energy filter with a bandwidth of 0.5 eV. By changing the kinetic energy (typically 0−500 eV) and the defocus, the image contrast can be optimized. While in the so-called bright-field mode the specularly reflected electrons are used for imaging, the dark-field mode utilizes the reflected electrons from a higher-order diffraction spot and therefore identifies superstructure domains or rotational domains.

We briefly sketch the crystal structures of the iron oxide phases with which we are concerned in our experiments, the main ones being FeO (wüstite), Fe_3O_4 (magnetite), and α-Fe_2O_3 (hematite) (see Figure 1). For a more detailed overview of these different crystalline structures see Weiss and Ranke.[15] α-Fe_2O_3 crystallizes in the corundum structure with a hexagonal unit cell. Along the [0001] direction the O anions form a close-packed hcp sublattice with ABAB stacking. The Fe^{3+} species between these layers are arranged in honeycomb ($\sqrt{3} \times \sqrt{3}$)R30° like layers. On an area of 12 O anions there are 8 Fe cations. Fe_3O_4 crystallizes in the inverse spinel structure. The O anions form a close-packed fcc sublattice with Fe^{2+} and Fe^{3+} cations located in the interstitial sites. Along the [111] axis of Fe_3O_4, the hexagonal O planes form a cubic ABC stacking sequence. The packing density of the O planes is similar to the O planes of α-Fe_2O_3. Between the close-packed planes of oxygen ions either one Kagomé or three hexagonal (mixtrigonal) Fe layers alternate. Both ion sublattices are arranged in a (2 × 2) like fashion on the close-packed oxygen layer. Here, 9 Fe cations are arranged on an area of 12 O anions. γ-Fe_2O_3 maghemite is a metastable phase with a cubic crystal structure close to the Fe_3O_4 magnetite structure. When Fe_3O_4 is oxidized to γ-Fe_2O_3, arbitrarily distributed cation vacancies are created at octahedral interstitials resulting in only Fe^{3+} cations. The so-called "nonstoichiometric magnetite"

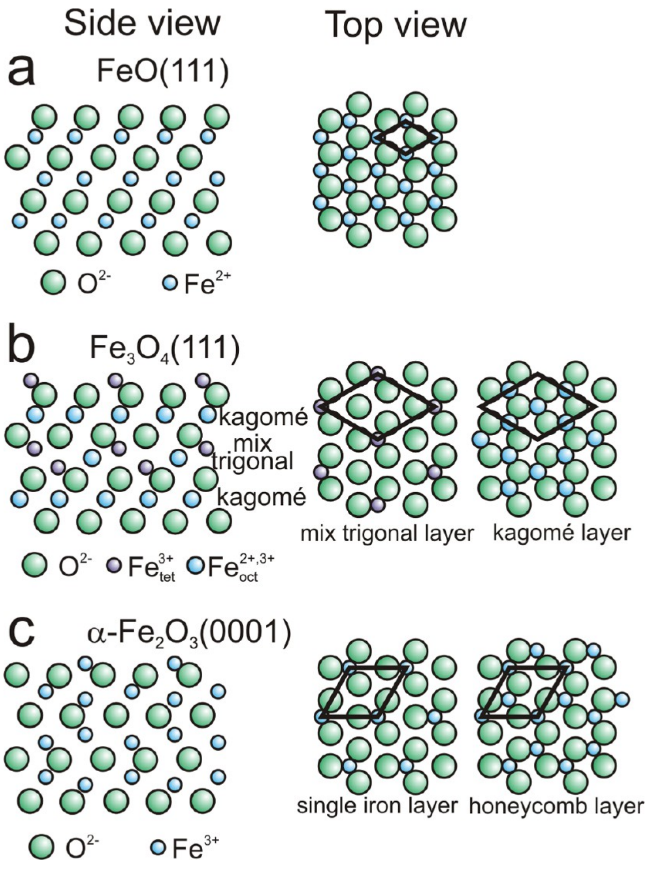

Figure 1. Crystal structures of FeO, wüstite (a), Fe_3O_4, magnetite (b), and α-Fe_2O_3, hematite. Oxygen and iron are represented as large green and small blue and violet balls. The different surface unit cells are added in the right part.

$Fe_{(3-\delta)}O_4$ (with $0 < \delta < 1/3$) describes the situation, when only part of these vacancies are formed ($\delta = 1/3$ corresponds to maghemite). In the FeO crystal structure, the O and Fe(111) planes form ideal two-dimensional hexagonal lattices with a cubic ABC stacking sequence along the [111] direction.

Pt(111) and Ag(111) crystals share an fcc bulk structure with similar interatomic distances of 2.77 and 2.89 Å, respectively. When iron oxide films are grown on them, they are oriented such that the close-packed oxygen layers are aligned as the Pt(111) and the Ag(111) substrates for both α-Fe_2O_3 and Fe_3O_4. While the $Fe_3O_4(111)$ surface exhibits in LEED an approximate (2 × 2) reconstruction—with respect to the Pt(111) surface structure—the α-$Fe_2O_3(0001)$ surface is characterized by an approximate $(\sqrt{3} \times \sqrt{3})R30°$ superstructure. The lattice constant of FeO(111) differs from that of the substrates by only 9.7% (Pt(111)) and 5.2% (Ag(111)), respectively, leading to typical Moiré patterns as significant fingerprints. All these three oxide structures grow in two rotational domains.[13,15]

Furthermore, α-Fe_2O_3 and Fe_3O_4 LEED patterns may exhibit extra hexagonal spots surrounding the main diffraction spot, indicating an additional long-range periodicity on the surface, the so-called biphase (α-Fe_2O_3[28] and Fe_3O_4[29]). The model for this periodic surface rearrangement is still under debate, and it is not clear if its origin is the same for both oxides.[29−31] In our work, the biphase was always present on α-Fe_2O_3 films (most likely due to our low oxygen pressure used for preparation), while for Fe_3O_4 films a biphase structure resulted if prepared by oxidation at lower temperature or by Fe deposition onto an α-Fe_2O_3 film at RT and subsequent annealing to 700 K. Under the conditions of our experiments, the initial $Fe_3O_4(111)$ surface is terminated by 1/4 of iron (in the following called "canonical"), as shown with LEED-IV and described in previous works.[7,9,32] By spatially resolved XPS and XPEEM, using the Fe^{2+} signal of the Fe 3p XPS peak, we could exclude that maghemite is present on our freshly prepared oxide films. We cannot exclude, however, that during conversion there is some change of the Fe:O ratio in the structurally Fe_3O_4-like regions since nonstoichiometric magnetite and maghemite have the same crystal structure and therefore the same LEED pattern.

Due to the low kinetic electron energy in our LEEM and LEED experiments (between 5 and 50 eV), our results are rather surface sensitive with a probing depth within 0.5−2 nm, which is only a fraction of our 10 nm thick oxide film. Therefore, with our experimental setup, we cannot directly exclude a layered film structure beyond our probing depth, such as α-Fe_2O_3 covered by Fe_3O_4 or a thick FeO layer at the interface to the Pt or Ag support. However, to our knowledge, no such scenario has been observed by other techniques. On the contrary, Willinger et al.[33] have recently reported on Fe_3O_4 films on Pt support, prepared under nearly identical conditions. Using HR-TEM, they found a homogeneous structure, from the surface to the interface. Therefore, we assume that the stable film structure, observed at the surface, represents the entire film thickness.

$Fe_3O_4(111)$ and α-$Fe_2O_3(0001)$ thin films were grown by repeated cycles of Fe deposition at RT (each cycle about 7−9 ML, where 1 ML Fe is the amount corresponding to one complete FeO layer on Pt(111)) and oxidation at elevated temperature, after one complete FeO layer was initially formed.[9] The final film thickness in our experiments was always 10 nm (±1 nm). On the Pt(111) surface, the $Fe_3O_4(111)$ film was produced by annealing at $T = 900$ K in $p = 1.0 \times 10^{-6}$ mbar oxygen, whereas α-$Fe_2O_3(0001)$ was formed at $T = 870$ K and $p = 3 \times 10^{-5}$ mbar. A lower oxidation temperature was used for the Ag(111) surface to avoid contamination from the bulk: Fe_3O_4 was formed at $T = 720$ K ($p_{O2} = 2 \times 10^{-6}$ mbar), while for α-$Fe_2O_3(0001)$ $T = 670$ K at $p = 2.4 \times 10^{-5}$ mbar was required. In spite of the different oxidation temperature, the oxide film morphology was nearly the same on both the Pt and the Ag substrate: a closed film with terrace width of a few tens of nanometers.

Under our preparation conditions we could usually find areas on the surface (for iron oxide films grown on both Pt(111) and Ag(111)) which were composed of domains of α-Fe_2O_3 and Fe_3O_4. We call these "mixed films". The two phases coexist for intermediate preparation parameters, often also showing small FeO domains due to partial dewetting.[9] In most cases discussed in the following, we started from such a mixed α-Fe_2O_3/Fe_3O_4 thin film, since this eased the observation of the conversions by LEEM. Whereas in the sections 3.1, 3.2, 3.4, and 3.5 only a small portion of 0.1% to 1% of the oxide film was α-Fe_2O_3, the majority of the film in section 3.3 had the hematite structure.

Figure 2 shows typical LEED patterns of the iron oxide films; the "mixed surface" (Figure 2d) is identified by the superposition of two single-phase LEED patterns of Fe_3O_4 and α-Fe_2O_3 (Figure 2b and c). The intensity of those LEED patterns as well as all others reported in the work are scaled logarithmically in order to emphasize the weaker superstructure and satellite spots. Selecting one of the significant LEED spots (labeled in Figure 2b and c) enables dark-field LEEM imaging to clearly identify different crystalline domains of the oxide films. The high k-resolution of our LEED mode enables the

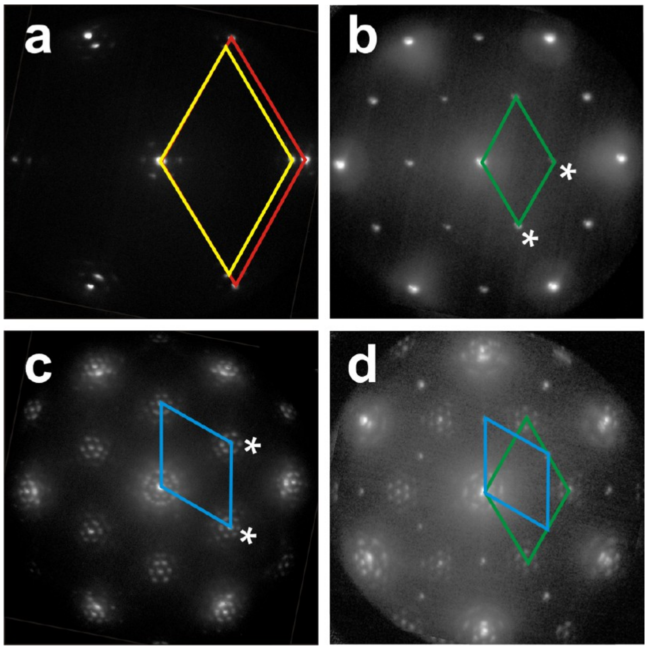

Figure 2. LEED patterns of the observed surface structures: (a) one layer of FeO on Pt(111) surface, (b) Fe_3O_4 film, and (c) α-Fe_2O_3 film with biphase structure. (d) "Mixed film": iron oxide film with coexisting domains of Fe_3O_4 and α-Fe_2O_3 biphase structures. Unit cells of Pt(111) (red), FeO (yellow), Fe_3O_4 (green), and α-Fe_2O_3 (blue) are indicated. The asterisks in (b) and (c) mark the significant spots selected for dark-field imaging to identify the corresponding structural domains. Electron energy $E_{kin} = 38$ eV is the same for all patterns.

study of spot profiles and shifts in spot position (SPA-LEED function).

3. RESULTS AND INTERPRETATION

3.1. Oxidation of Magnetite: $Fe_3O_4 + O_2 \rightarrow \alpha\text{-}Fe_2O_3$.

Oxidation of the Fe_3O_4 surface, supported by a Pt(111) substrate, to α-Fe_2O_3 was studied by directly monitoring the behavior of a mixed film upon annealing in O_2 pressure, as shown in the sequence in Figure 3. The initial surface (Figure 3a) consists of the two main domains, easily distinguishable by their strong contrast—bright for the Fe_3O_4 and dark for the α-Fe_2O_3 area; in the latter domain FeO holes are additionally visible. The film was annealed in 3×10^{-5} mbar O_2 pressure, starting at RT up to 700 K. Figures 3(b–i) show the surface evolution during the experiment. During the initial annealing, at about 500 K, the LEEM intensity of the Fe_3O_4 area is reduced, which causes a contrast inversion between Figures 3(a) and (b). This is related to a structural change on the Fe_3O_4 surface; most likely, the Fe termination switches to an oxygen-rich termination, as observed recently by Sala et al.[9]

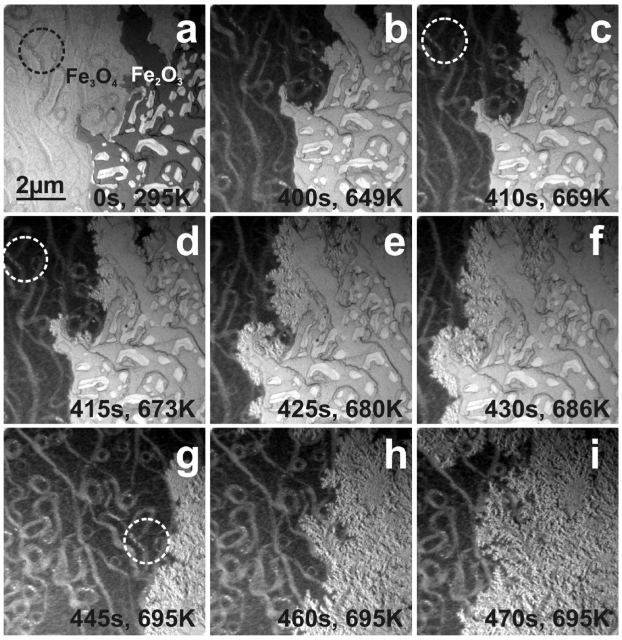

Figure 3. Oxidation of a mixed iron oxide film at $p_{O2} = 3 \times 10^{-5}$ mbar in the temperature range between RT and 700 K. Initial surface (a) consists of α-Fe_2O_3 (dark) and Fe_3O_4 (bright) areas and, additionally, of FeO holes (bright) in the α-Fe_2O_3 region. The reaction front between α-Fe_2O_3 and Fe_3O_4 starts moving at 670 K (c). Between (f) and (g) the sample was shifted to follow the conversion front. The circle, marking the identical surface spot, is meant as a help for the eye. The image contrast is inverted from (a) to (b) due to structural changes at the α-Fe_3O_4 surface. Image intensity is scaled to minimum/maximum in all images to optimize the contrast, E_{kin} = 20 eV.

At 670 K (Figure 3c) the α-Fe_2O_3 domain starts to grow into the Fe_3O_4 phase with a growth front of dendritical shape. The process becomes faster when the temperature is increased up to 700 K (Figure 3g). While at 680 K the front moves with a velocity of about 40 nm/s from the right to the left, the velocity is 150 nm/s at 695 K, indicating that the transformation process is thermally activated.[34]

During annealing, FeO domains in the α-Fe_2O_3 area increase in size, as observed before in connection with the Fe_3O_4 thin films.[9] This is associated with a dewetting of the oxide film itself, forming deep holes down to the substrate, which are filled with (most likely only) one monolayer thin FeO layer as proven by XPEEM.

3.2. Annealing of Magnetite on a Pt Substrate: $Fe_3O_4 \rightarrow \alpha\text{-}Fe_2O_3$.

For annealing in low pressure the bulk P–T phase diagram[15,36,35] suggests the reduction of the iron oxide film from α-Fe_2O_3 to Fe_3O_4. The sequence (a) to (i) in Figure 4 shows the annealing behavior of an α-Fe_2O_3 domain surrounded by Fe_3O_4 in a temperature range between RT and 950 K. The initial surface (Figure 4a) at RT consists of two domains with strong contrast. Dark-field images—utilizing the specific LEED spots of each structure—confirm that the central dark domain is an α-Fe_2O_3 domain, whereas the remaining part has the crystal structure of Fe_3O_4.

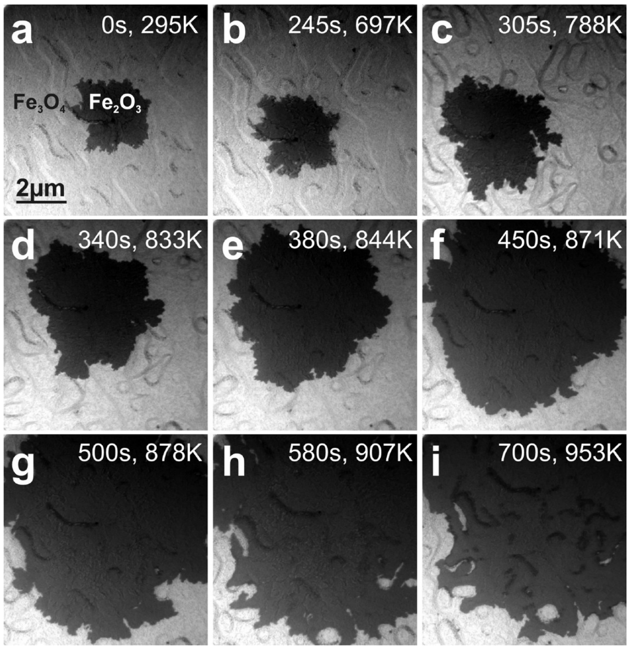

Figure 4. Annealing of a mixed iron film on a Pt(111) substrate in UHV. Fe_3O_4 (bright) transforms into α-Fe_2O_3 (dark). FeO holes (black) get enlarged above 850 K (f). Annealing time and temperature are given in each image. E_{kin} = 29 eV.

Upon annealing in UHV, the conversion starts at about 697 K (Figure 4b). The transformation front exhibits a dendritical shape. This front is influenced by the overall film morphology: step bunches, caused by the substrate underneath and appearing as dark gray, wavy and round lines, and FeO holes may slow down or even block the migration of the growth front. A rough estimate of the average speed of the growth front reveals a noncontinuous temperature dependence; whereas at 855 K (Figure 4e,f) the front migrates with about 30 nm/s, and the speed is 2/3 of that value at 800 K (Figure 4c) and above 870 K (Figure 4g). Above 900 K (Figure 4h,i) the FeO area (black in the images) increases in size, again corresponding to a dewetting of the α-Fe_2O_3 film—which is expected on this time scale for this high temperature and a film thickness of 10 nm. We note that even if the initial surface had a uniform structure (i.e., no mixed domains) within the observed area we never observed a homogeneous transformation. Instead a huge and fast front was then seen, crossing the observed field of view.

Clearly, the experimentally observed transformation is just the opposite of what is expected from the phase diagram for stable bulk iron oxides.[36] Also, Schlueter et al. found the inverse result; i.e., α-Fe_2O_3 transforms to Fe_3O_4 upon annealing by oxygen desorption, but on a different substrate, namely, on Ag(111).[13] We corroborated this with our methods as well (see section 3.4).

So here the ratio Fe:O was not changed by oxygen desorption but by a decrease of the Fe concentration: Fe must disappear from the oxide layer. As will be discussed below, iron likely diffuses toward the interface between Pt support and oxide film, either increasing the Fe concentration at the interface or being dissolved in the Pt(111) substrate.

In the following, we intentionally increased the Fe concentration by deposition to enforce the inverse transformation.

3.3. Fe Deposition on Hematite: α-Fe_2O_3 + Fe → Fe_3O_4. When we used Pt(111) to support the iron oxide film, we have never observed the reduction of the α-Fe_2O_3 film by thermal desorption of oxygen. We could, however, intentionally reduce α-Fe_2O_3 by adding iron to the α-Fe_2O_3 film, thus increasing the Fe:O ratio. For this purpose, 3 ML of iron was deposited at RT on an initially complete α-Fe_2O_3 film with biphase structure (LEEM and LEED in Figure 5(a) and (d), respectively); only a few FeO holes (bright in Figure 5a) were visible, aligned along the step bunches of the substrate. The Fe deposition changed the image intensity homogeneously; i.e., no domains were visible. After Fe deposition, LEED showed a rather disordered structure and contained only the central (00) spot and weak spots originating from the oxygen layers but neither the biphase structure nor spots related to the specific Fe termination (no quasi $(\sqrt{3} \times \sqrt{3})R30°$ superstructure spots). Subsequently, the substrate temperature was increased in UHV from RT to 700 K within 5 min and held at that temperature for 90 s, before cooling down to RT again. Finally, in a second annealing process, the temperature was raised to 800 K within 5 min and kept for 100 s. Both deposition and annealing were observed in *real time* in LEEM.

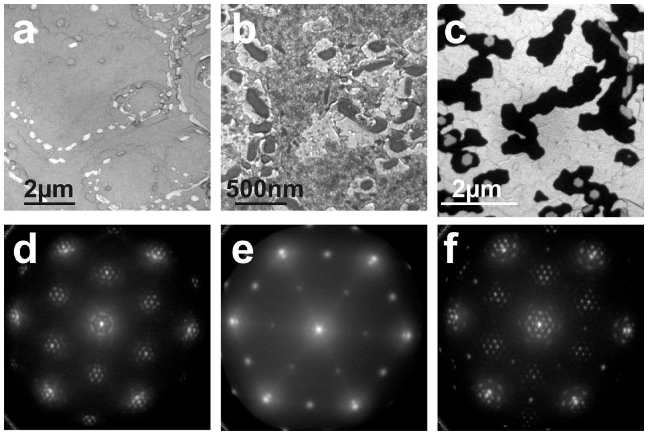

Figure 5. Reduction of the α-Fe_2O_3 film by Fe deposition at RT and subsequent annealing in UHV. (a)+(d): LEEM image and LEED pattern of the initial α-Fe_2O_3 surface at RT before Fe deposition: FeO holes appear bright; E_{kin} = 38 and 40 eV, respectively. (b)+(e) The same surface covered with 3 ML of Fe and annealed to 700 K; FeO holes (dark) are surrounded by Fe_3O_4 with canonical termination; the rest of the surface shows an "intermediate biphase"; LEEM at E_{kin} = 27 eV and LEED at E_{kin} = 41 eV. (c)+(f) Surface after a further annealing at 800 K; Fe_3O_4 (dark) with canonical termination in the vicinity of FeO holes (gray) and α-Fe_2O_3 biphase (bright); LEEM at E_{kin} = 24 eV and LEED at E_{kin} = 41 eV. The surface areas in (a)−(c) are not identical due to thermal drift.

During the first annealing, the reduction of the hematite surface to magnetite occurred in two steps: first, the surface intensity changed uniformly around T = 570 K within approximately 20 s, indicating the formation of a different homogeneous, most likely Fe-terminated surface. In a second step, areas with different contrast were formed, preferentially surrounding the FeO holes (light areas around the dark FeO holes in Figure 5b, corresponding LEED pattern in Figure 5e). At T = 700 K the formation of these domains was completed after 90 s, and the sample was cooled to RT.

Dark-field LEEM imaging using the significant LEED superstructure spots for α-Fe_2O_3, Fe_3O_4, and biphase showed that the initial α-Fe_2O_3 surface was almost completely reduced. The resulting surface (Figure 5b) has two different terminations clearly distinguishable in LEEM: a "canonical magnetite" phase[9] with a pure (2 × 2) LEED pattern (bright domains in Figure 5b), mainly located nearby FeO holes (dark), and an unusual surface termination (gray), which covers the majority of the surface.

The LEED pattern of the latter termination consists of the (00) and first-order spots, showing long-range order of the oxygen layer, both surrounded by extra spots similar to those of the biphase-terminated iron oxides (with a periodicity of 4−6 nm). Remarkably, neither the (2 × 2) nor the $(\sqrt{3} \times \sqrt{3})R30°$ superstructure is visible, indicating either a (1 × 1) arrangement of the Fe layer with respect to the oxygen layer or disordered Fe layers. This up to now unknown termination needs further investigation. It will be called "intermediate biphase" in the following. The thermal stability of this Fe_3O_4 film was tested by a second annealing in UHV, this time from RT to 800 K. While regions exhibiting the canonical Fe_3O_4 structure did not change, the "intermediate biphase" region was quickly converted to the α-Fe_2O_3 structure at T = 710 K. This annealing was stopped after all "intermediate biphase" areas were fully converted to α-Fe_2O_3. The LEEM image and the LEED pattern of the final film are shown in Figure 5c and 5f, respectively. At the used electron energy, the canonical Fe_3O_4 structure appears dark in the image, the FeO covered holes gray, and the α-Fe_2O_3 bright, as corroborated by dark-field imaging. The related LEED pattern consists of a superposition of a strong "$(\sqrt{3} \times \sqrt{3})R30°$" with satellite spots for the biphase α-Fe_2O_3 structure and a weaker "2 × 2" like Fe_3O_4 pattern.

3.4. Annealing of Magnetite on a Ag Substrate: Fe_3O_4 → α-Fe_2O_3. As pointed out in section 3.2, the observed conversion of Fe_3O_4 to α-Fe_2O_3 by annealing in UHV clearly contradicts the phase diagram of equilibrium bulk iron oxide and experimental observations on thin film growth of iron oxides on Ag(111).[13] We therefore repeated the annealing experiment on a Ag(111) substrate, in order to elucidate the role of the substrate.

A mixed α-Fe_2O_3/Fe_3O_4 film was prepared on a Ag(111) surface, using the recipe described above, yielding a complete iron oxide film. The comparison of our SPA-LEED data, taken of iron oxide films grown on Pt(111) and Ag(111) substrates, shows significant differences for the periodicity of the Moiré patterns of the atomically thin FeO layer on Pt(111) and on Ag(111), which can be easily explained by the different lattice mismatch between the FeO film and the two substrates. On the

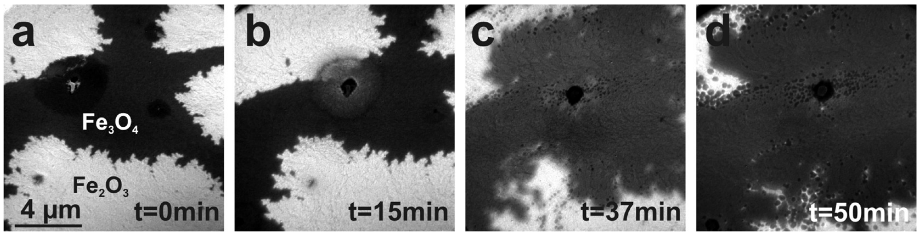

Figure 6. Reduction of the α-Fe$_2$O$_3$ film by annealing at $T = 823$ K in UHV, observed on a Ag(111) surface. (a) The initial surface with α-Fe$_2$O$_3$ and Fe$_3$O$_4$ areas. The central dark dot is a defect on the surface and can be used as a reference point. Annealing time is given on each image. $E_{\mathrm{kin}} = 24$ eV.

other hand, the periodicity of the α-Fe$_2$O$_3$ biphase is identical on both substrates. Therefore, the biphase periodicity is related to a superficial reconstruction and is not caused by a possible strain in the iron oxide film due to lattice misfit to the substrate.

This mixed film was annealed in UHV from RT to $T = 823$ K and kept nearly 1 h at this temperature. The process was observed in real time with LEEM (Figure 6). After 20 min of annealing, the domain boundaries between α-Fe$_2$O$_3$ and Fe$_3$O$_4$ start moving (compare Figure 6b and c), transforming α-Fe$_2$O$_3$ into Fe$_3$O$_4$. This transformation upon annealing, related to desorption of oxygen, is expected from the phase diagram of bulk iron oxides and agrees with the experimental finding of others.[13] Compared to the annealing processes of iron oxide films on the Pt(111) substrate, the speed of the front is much slower for the Ag(111) substrate: whereas the observed fronts on the Pt(111) substrate move with a velocity of up to 16 nm/s, the velocity on the Ag(111) surface is 1 order of magnitude smaller, about only 1 nm/s.[34]

3.5. XPS and XPEEM Results: Fe Valency in the Oxide Films and Fe Solution in Pt.

While the spatial and temporal resolution of our XPEEM setup is not sufficient to follow in real-time the described structural conversions seen by LEEM, static images after quenching were possible. So some additional information could be obtained by XPS and XPEEM. The first concerns the valency of the iron in the layers, and the second supports the interpretation given in section 3.2 that heating of Fe$_3$O$_4$ films on Pt in UHV leads most likely to dissolution of Fe in the Pt substrate.

Because the LEED patterns of Fe$_3$O$_4$ and γ-Fe$_2$O$_3$ are identical, this method cannot distinguish between these two phases. However, spatially resolved XPS, generated from an energy stack of XPEEM images, using the Fe^{2+} signal, is sensitive to this transformation. This has been demonstrated for experiments on the low-temperature oxidation of Fe$_3$O$_4$ to γ-Fe$_2$O$_3$ at 570 K, both in LEEM/LEED and XPEEM (article in preparation). In this work LEEM saw strong structural contrast for the resulting mixed γ-/α-Fe$_2$O$_3$ film, whereas, on the other hand, XPEEM does not show any contrast in the Fe composition: for both phases we found only Fe^{3+}, as expected. Using the same approach in the present connection on the partially transformed Fe$_3$O$_4$ films annealed to the higher temperature in UHV given in section 3.3 and then cooled to room temperature to have stable conditions, the comparison of spatially resolved XPS from α-Fe$_2$O$_3$ and surrounding Fe$_3$O$_4$ areas exhibited a reduced, but still existing, Fe^{2+} signal. The signal strength was not sufficiently reproducible to draw quantitative conclusions, but we can safely conclude that under these conditions the film has Fe$_3$O$_4$ structure with reduced concentration of Fe^{2+} cations (also called "non-stoichiometric magnetite"). So this state precedes the structural transformation and not maghemite (without any Fe^{2+}).

In section 3.2 we have mentioned that the observed unexpected UHV conversion of Fe$_3$O$_4$ films may be explainable by solution of Fe in the Pt substrate. The fact that this process does not occur with Ag-supported Fe$_3$O$_4$ films is support for this interpretation since Ag does not dissolve Fe[37] while Pt does.[38] Further evidence comes from XPS and LEED: neither did XPS show any enrichment of Fe on the surface nor did LEED indicate a structural change, by, e.g., changing the superstructure or spot broadening. The only alternative we can see is Fe diffusion to the substrate, where it can easily be dissolved.[39] This is not a novel proposal; it has also been suggested by Morrall et al. to explain their observation of nonstoichiometric Fe$_3$O$_4$ films.[40] Further observations support this explanation. After the experiments and a first cleaning of the sample, a FeO layer formed on the Pt surface in an oxygen atmosphere, even though no Fe had been deposited before. We conclude that Fe segregates out of the Pt bulk in oxygen (as is well-known for C on W(110) in an oxygen atmosphere). By repeated cycles of sputtering and oxidation, we could get rid of this Fe dissolved in the Pt bulk (probably close to the surface); the FeO layer then did not form anymore in the oxygen atmosphere. For the film experiments we used only these depleted Pt substrates, cleaned from dissolved Fe by oxygen treatment. Also, if on such a surface an FeO layer was prepared by deposition of 1 ML at RT (RT to avoid dissolution) and annealing in oxygen atmosphere, this FeO layer decomposed by annealing above 1100 K in UHV, and Fe dissolved in the Pt bulk, as checked by subsequent annealing in oxygen and the observed formation of FeO. From all this, we conclude that the Fe dissolution in the Pt substrate is most likely not just a consequence of the cleaning process (selective sputtering of the iron oxide film) but occurs during the annealing processes and transformations.

4. DISCUSSION

We investigated the transformations between Fe$_3$O$_4$(111) and α-Fe$_2$O$_3$(0001) thin films grown on Pt(111) and Ag(111) surfaces under different driving forces and their reversibility conditions. The transformation processes are driven either by oxidation, by annealing in UHV, or by Fe deposition with subsequent annealing. In most cases, the initial film was prepared such that it was composed by both structures since this eased the observation of the conversions. The phase transformations were not uniform but proceeded via a growth front, such that one kind of structural domain increased in size and the other one shrunk.

For a deeper understanding of the phase transitions, the differences in the crystal structures of hematite (α-Fe$_2$O$_3$) and magnetite (Fe$_3$O$_4$) must be considered. The main differences between the two iron oxide structures are (i) the Fe density in a ratio Fe (in α-Fe$_2$O$_3$):Fe (Fe$_3$O$_4$) of 8:9 (whereas the two-dimensional O density is the same); (ii) the structure of the Fe sublattices; and finally (iii) the stacking of the close-packed oxygen planes. As a consequence, a phase transformation involves a change in the Fe density and concomitantly of the Fe:O ratio, as well as structural rearrangements in the Fe sublattice and in the stacking of the close-packed oxygen planes. The spinel forming process, as well as the spinel to corundum transformation, have been extensively studied in solid−solid reactions, pointing out the role of cation diffusion and crystalline rearrangement. The restacking of the oxygen layers is believed to progress through rigid O layers shifting against each other which induces the simultaneous adjustment of cations in the new structure, as discussed in Kachi et al.,[41] in Carter and Schmalzried,[42] and more generally by Schmalzried.[43]

A frame of rigid O-layers, providing sites for cation rearrangements, is used also in a model for the spinel forming process from binary oxides by Hesse.[44] Here, the diffusion and the rearrangement of the cations drive the transformation: in our case the Fe diffusion at the transformation of Fe_3O_4 to γ-Fe_2O_3. This conversion might occur as an intermediate step during our annealing experiment since the structures of these oxides are indistinguishable in our experiments. In a final step, this γ-Fe_2O_3 structure might transform to α-Fe_2O_3, as observed experimentally and described theoretically by Kachi et al.[41]

However, this two-step model can only be applied with constraints to our observations in section 3.2. The XPS results reported in section 3.5 show that the entire Fe_3O_4 area is not completely converted to a γ-Fe_2O_3 structure before being transformed to α-Fe_2O_3 because after cooling the unconverted area still showed an Fe^{2+} signal in XPS, indicating at least a nonstoichoimetric magnetite structure. However, during the conversion, there might be a vertical and/or horizontal gradient in the Fe concentration of the magnetite area, yielding in a γ-Fe_2O_3 region at the moving conversion front to α-Fe_2O_3, meaning indeed a local two-step process from Fe_3O_4 via γ-Fe_2O_3 to α-Fe_2O_3. To finally describe the spatial-temporal evolution of the conversion, the system has to be investigated in more detail combining structural and spectroscopic contrast at reaction conditions.

Starting with a mixed surface of different structural domains, the film is converted by a moving reaction front. The velocity of the front depends on temperature; therefore, the transformation must be driven by thermally activated processes. This is expected for all processes necessary for conversion: (i) density change of Fe, (ii) structural rearrangement of the Fe sublattices, and (iii) modification of the close-packed oxygen layer stacking. In order to reduce the Fe density, Fe cations have to diffuse through the iron oxide film along the [111] direction. This Fe diffusion is assumed to proceed by interstitial collinear removal.[45,46] When these Fe cations diffuse to the surface, they react with oxygen from the gas phase. Thus, after completion of the oxidation process, the iron oxide film has grown in thickness, because 1/9 of the Fe cations of the initial Fe_3O_4 domains have diffused to the surface. The velocity of the transformation front of 150 nm/s at 700 K and $p_{O2} = 3 \times 10^{-5}$ mbar is the highest observed in our experiments, and therefore oxidation is completed within only a few minutes, as already observed by Schlueter[13] on a Ag(111) surface. We conclude that the activation barriers for the oxidation must be lower than for the competing processes (see below).

An interesting observation is the dendrite shape of the front. Most likely the conversion process at 700 K is defect-dominated, leading to imperfect stacking or rearrangement of the Fe sublattice, so that the conversion occurs locally (see Figure 3). In contrast to Nie et al.,[47] we have not observed the formation of Fe_3O_4 domains within the α-Fe_2O_3 phase, far away from the oxidation front, and therefore we exclude a reaction like $9Fe_3O_4 + 2O_2 \rightarrow 12Fe_2O_3 + Fe_3O_4$. The reason for the difference might be their film thickness of 100 nm, in contrast to 10 nm in our experiments.

For a mixed film on Ag(111), the expected reduction behavior α-$Fe_2O_3 \rightarrow Fe_3O_4$ was observed, in agreement with previous work.[13] Though the annealing was carried out at higher temperature (823 K) the process was very slow. The full conversion needed more than an hour, corresponding to a speed of the conversion front of only 1 nm/s. Here, the process is most likely driven by overcoming the attractive potential between Fe and O at the surface and the subsequent α-Fe_2O_3 desorption of oxygen and diffusion of Fe into the oxide layer, where it is incorporated in the interstitial Fe layers.

As stressed above, the behavior observed when a mixed film on Pt(111) was annealed in UHV was definitely unexpected. Instead of the expected reduction process the opposite transformation occurs: Fe_3O_4 transforms to α-Fe_2O_3. Here the conversion front has a speed of 30 nm/s (maximum at about 855 K). Because no additional oxygen was offered to the system, the ratio of Fe:O can be only lowered, if the Fe cations diffuse either to the surface or to the oxide−Pt interface. As stated in section 3.5 we can exclude Fe enrichment at the surface. Therefore, the segregated iron might form an FeO layer at the interface. In this model, the entire conversion would transform the topmost 3/4 of the initial Fe_3O_4 area to α-Fe_2O_3, the bottom part to FeO, corresponding to a reaction $Fe_3O_4 \rightarrow Fe_2O_3 + FeO$. Alternatively, Fe may diffuse into the Pt substrate, where it can be easily dissolved. In our case of a 10 nm thick Fe_3O_4 film the total diffused amount of Fe cations corresponds to ∼3.3 ML in the corresponding domains.

The Fe dissolution can explain the opposing results obtained on the two substrates Pt and Ag. The reason is the different behavior of the substrates: Fe can be dissolved in the Pt bulk, but not in the Ag bulk.[37,38] The desorption of oxygen (the dominant process on the Ag(111) substrate) must occur as well on the Pt substrate, but at a much slower rate than Fe segregation into the substrate. However, oxygen desorption might explain why the front velocity on the Pt substrate decreases at higher temperature.

Another type of transformation is initiated by Fe deposition and therefore by a forced enrichment of Fe density. This process converts α-Fe_2O_3 into Fe_3O_4 and also needs thermal activation. At 700 K the conversion is incomplete: only 20% of the surface converts to canonical Fe_3O_4, and the remaining part shows an (up to now unreported) "intermediate biphase". The conversion may be explained by diffusion of deposited Fe into the oxide film. Compared to the oxidation of Fe_3O_4, this process takes more time because iron diffusion is less favored in α-Fe_2O_3 than in Fe_3O_4.[45,46,48] A second annealing to 800 K reconverts the "intermediate biphase" to α-Fe_2O_3. However, when we repeated the experiment and added this time 10 ML of Fe, the film was fully converted and stable upon higher annealing, indicating that it is necessary to add a sufficient amount of Fe to complete the transformation throughout the film.

We finally return to the observation that all transformations occurred with growth fronts. For mixed films this is shown in Figures 3, 4, and 6. As mentioned in section 3.2, even for an initially uniform surface we never observed a homogeneous transformation, but a huge, fast front was then eventually crossing the observed field of view. Obviously, the transformations are promoted by nucleation centers. Once a favored domain has formed (or pre-exists in the mixed films), the transformation continues by growing in size, i.e., with a moving front. We never observed a spontaneous phase transformation on a homogeneous surface (neither for α-Fe_2O_3 nor Fe_3O_4) but only at the front between two phases. Obviously, the transformation to Fe_3O_4 needs a seed to start. The LEEM observations show that most of the seeds are formed in the vicinity of micrometer-large, mesa-like morphological defects of the metal support, as they always existed on our substrate.

As to the nature of the observed moving growth fronts during conversions, it should be borne in mind that the contrast in LEEM is due to the geometry change between Fe_3O_4 and α-Fe_2O_3. The direct role of the front—whether the Fe diffusion or oxygen diffusion occurs only at the border between two phases, or nearby, or independently—cannot be answered from our present experiments because our XPEEM setup lacks the temporal and spatial resolution required for this. However, it is well possible that the front motion is not connected to material diffusion of O and/or Fe but to “diffusion” of an activated structural arrangement between the two phases. The changes of Fe:O ratio driving these structural conversions could well occur on a faster time scale and possibly be even laterally homogeneous over the film. The structural change would then be slower because it can occur only at the mentioned seeds and propagate by a repeatable step. We hope to gain further insight from ongoing investigations.[34]

5. CONCLUSIONS

This paper describes a study on the transformations between hematite and magnetite in thin films on Pt(111) and on the Ag(111) substrate, using mainly LEEM and LEED complemented by XPS and XPEEM. The transformations involve both structural changes of the oxygen and iron layers and a change in the Fe concentration and might be explained by a two-step process via an intermediate maghemite or nonstoichiometric magnetite phase. The conversions appear to be mainly driven by the interstitial diffusion of iron in the film. In the case of the oxidation of Fe_3O_4 to α-Fe_2O_3, Fe has to diffuse from the film to the surface, where it is oxidized. For the reduction by oxygen desorption, observed on Ag(111), the reverse process occurs: breaking the Fe−O bond at the surface and diffusion of Fe into the oxide film. The enrichment of Fe density by Fe deposition and annealing leads to a reduction process as well: α-$Fe_2O_3 \rightarrow Fe_3O_4$. A novel additional process is the decrease of the Fe:O ratio by Fe diffusion toward the supporting interface, most likely into the substrate bulk, possible only on the Pt(111) substrate, but not on Ag(111). This leads to an unexpected “oxidizing” process on the Pt(111), though no oxygen is added to the oxide film, but the Fe density is reduced. This observation stresses the possible importance of the substrate for supported thin oxide films. All processes are thermally activated and promoted by nucleation centers. The transformations are not homogeneous but take place with conversion fronts which move at considerably different rates and with complicated morphology and which deserve further study.

AUTHOR INFORMATION

Corresponding Author

*E-mail: thomas.schmidt@fhi-berlin.mpg.de. Phone: +49-30-8062-1-4671.

Notes

The authors declare no competing financial interest.

ACKNOWLEDGMENTS

We gratefully acknowledge the financial support by the Federal German Ministry of Education and Science (BMBF) under Contract no. 05KS4WWB/4, the German Science Foundation (DFG) through Sonderforschungsbereich 546, and the Cluster of excellence UNICAT, as well as Fonds der Chemischen Industrie. We are thankful for the technical support by the BESSY-II crew. The microscope is installed at the BESSY-II storage ring of the Helmholtz-Center Berlin for Material and Energy. We thank HZB for the allocation of synchrotron radiation beamtime.

REFERENCES

(1) Cornell, R. M.; Schwertmann, U. *The Iron Oxides*; Wiley-VCH: Weinheim, Germany, 2003.

(2) Ertl, G.; Knözinger, H.; Schüth, F.; Weitkamp, J. *Handbook of Heterogeneous Catalysis*; Wiley-VCH: Weinheim, Germany, 2008.

(3) Yue, J.; Jiang, X.; Kaneti, Y. V.; Yu, A. Experimental and Theoretical Study of Low-Dimensional Iron Oxide Nanostructures. In *Smart Nanoparticles Technology*; Hashim, A., Ed.; InTech: Rijeka, 2012; pp 119−146.

(4) Zboril, R.; Mashlan, M.; Petridis, D. Iron(III) Oxides from Thermal Processess Synthesis, Structural and Magnetic Properties, Mössbauer Spectroscopy Characterization, and Application. *Chem. Mater.* **2002**, *14*, 969−982.

(5) Vurens, G. H.; Salmeron, M.; Somorjai, G. A. Structure, Composition and Chemisorption Studies of Thin Ordered Iron Oxide Films on Platinum (111). *Surf. Sci.* **1988**, *201*, 129−144.

(6) Weiss, W.; Ritter, M. Metal Oxide Heteroepitaxy: Stranski-Krastanov Growth for Iron Oxides on Pt(111). *Phys. Rev. B* **1999**, *59*, 5201−5213.

(7) Ritter, M.; Weiss, W. Fe_3O_4(111) Surface Structure Determined by LEED Crystallography. *Surf. Sci.* **1999**, *432*, 81−94.

(8) Lennie, A. R.; Condon, N. G.; Leibsle, F. M.; Murray, P. W.; Thornton, G.; Vaughan, D. J. Structures of Fe_3O_4 (111) Surfaces Observed by Scanning Tunneling Microscopy. *Phys. Rev. B* **1996**, *53*, 10244−10253.

(9) Sala, A.; Marchetto, H.; Qin, Z.-H.; Shaikhutdinov, S.; Schmidt, Th.; Freund, H.-J. Defects and Inhomogeneities in Fe_3O_4(111) Thin Film Growth on Pt(111). *Phys. Rev. B* **2012**, *86*, 155430−1−155430−10.

(10) Karunamuni, J.; Kurtz, R. L.; Stockbauer, R. L. Growth of Iron Oxide on Cu(001) at Elevated Temperature. *Surf. Sci.* **1999**, *442*, 223−238.

(11) Xue, M.; Wang, S.; Ku, K.; Guo, J.; Guo, Q. Surface Structural Evolution in Iron Oxide Thin Films. *Langmuir* **2011**, *27*, 11−14.

(12) Waddill, G. D.; Ozturk, O. Epitaxial Growth of Iron Oxide Films on Ag(111). *Surf. Sci.* **2005**, *575*, 35−50.

(13) Schlueter, C.; Lübbe, M.; Gigler, A. M.; Moritz, W. Growth of Iron Oxides on Ag(111) — Reversible Fe_2O_3/Fe_3O_4 Transformation. *Surf. Sci.* **2011**, *605*, 1986−1993.

(14) Deng, X.; Lee, J.; Matranga, C. Preparation and Characterization of Fe_3O_4(111) Nanoparticles and Thin Films on Au(111). *Surf. Sci.* **2010**, *604*, 627−632.

(15) Weiss, W.; Ranke, W. Surface Chemistry and Catalysis on Well-Defined Epitaxial Iron-Oxide Layers. *Prog. Surf. Sci.* **2002**, *70*, 1−151.

(16) Wang, X.-G.; Weiss, W.; Shaikhutdinov, Sh. K.; Ritter, M.; Petersen, M.; Wagner, F.; Schlögl, R.; Scheffler, M. The Hematite (α-

Fe_2O_3) (0001) Surface: Evidence for Domains of Distinct Chemistry. *Phys. Rev. Lett.* **1998**, *81*, 1038−1041.

(17) Kuhlenbeck, H.; Shaikhutdinov, S.; Freund, H.-J. Well-Ordered Transition Metal Oxide Layers in Model Catalysis - A Series of Case Studies. *Chem. Rev.* **2013**, *113*, 3986−4034.

(18) Monti, M.; Santos, B.; Mascaraque, A.; Rodriguez de la Fuente, O.; Nino, M. A.; Mentes, T. O.; Locatelli, A.; McCarthy, K. F.; Marco, J. F.; de la Figuera, J. Oxidation Pathways in Bicomponent Ultrathin Iron Oxide Films. *J. Phys. Chem. C* **2012**, *116*, 11539−11547.

(19) Tang, Y.; Qin, H.; Wu, K.; Guo, Q.; Guo, J. The Reduction and Oxidation of Fe_2O_3(0001) Surface Investigated by STM. *Surf. Sci.* **2013**, *609*, 67−72.

(20) Colombo, U.; Fagherazzi, G.; Gazzarrini, F.; Lanzavecchia, G. Mechanisms in the First Stage of Oxidation in Magnetites. *Nature* **1964**, *202*, 175−176.

(21) Gallagher, K. J.; Feitknecht, W.; Mannweiler, U. Mechanism of Oxidation of Magnetite to γ-Fe_2O_3. *Nature* **1968**, *217*, 1118−1121.

(22) Colombo, U.; Fagherazzi, G.; Gazzarrini, F.; Lanzavecchia, G. Mechanism of Low Temperature Oxidation of Magnetites. *Nature* **1968**, *219*, 1036−1037.

(23) Feitknecht, W.; Gallagher, K. J. Mechanisms for the Oxidation of Fe_3O_4. *Nature* **1970**, *228*, 548−549.

(24) Freund, H.-J. Metal-Supported Ultrathin Oxide Film Systems as Designable Catalysts and Catalyst Supports. *Surf. Sci.* **2007**, *601*, 1438−1442.

(25) Fink, R.; Weiss, M. R.; Umbach, E.; Preikszas, D.; Rose, H.; Spehr, R.; Hartel, P.; Engel, W.; Degenhardt, R.; Kuhlenbeck, H.; et al. SMART: A Planned Ultrahigh-Resolution Spectromicroscope for BESSY II. *J. Electron Spectrosc. Relat. Phenom.* **1997**, *84*, 231−250.

(26) Schmidt, Th.; Marchetto, H.; Lévesque, P. L.; Groh, U.; Maier, F.; Preikszas, D.; Hartel, P.; Spehr, R.; Lilienkamp, G.; Engel, W.; et al. Double Aberration Correction in a Low-Energy Electron Microscope. *Ultramicroscopy* **2010**, *110*, 1358−1361.

(27) Freund, H.-J.; Nilius, N.; Risse, T.; Schauermann, S.; Schmidt, Th. Innovative Measurement Techniques in Surface Science. *Chem. Phys. Chem.* **2011**, *12*, 79−87.

(28) Lad, R. J.; Henrich, V. E. Structure of α-Fe_2O_3 Single Crystal Surfaces Following Ar^+ Ion Bombardment and Annealing in O_2. *Surf. Sci.* **1988**, *193*, 81−93.

(29) Condon, N. G.; Leibsle, F. M.; Lennie, A. R.; Murray, P. W.; Vaughan, D. J.; Thornton, G. Biphase Ordering of Iron Oxide Surfaces. *Phys. Rev. Lett.* **1995**, *75*, 1961−1964.

(30) Condon, N. G.; Leibsle, F. M.; Parker, T.; Lennie, A. R.; Vaughan, D. J.; Thornton, G. Biphase ordering on Fe_3O_4(111). *Phys. Rev. B* **1997**, *55*, 15885−15894.

(31) Lanier, C. H.; Chiaramonti, A. N.; Marks, L. D.; Poeppelmeier, K. R. The Fe_3O_4 Origin of the "Biphase" Reconstruction on α-Fe_2O_3(0001). *Surf. Sci.* **2009**, *603*, 2574−2579.

(32) Barbieri, A.; Weiss, W.; Van Hove, M. A. Magnetite Fe_3O_4(111): Surface Structure by LEED Crystallography and Energetics. *Surf. Sci.* **1994**, *302*, 259−279.

(33) Willinger, M. G.; Zhang, W.; Bondarchuk, O.; Shaikhutdinov, S.; Freund, H.-J.; Schlögl, R. A Case of Strong Metal−Support Interactions: Combining Advanced Microscopy and Model Systems to Elucidate the Atomic Structure of Interfaces. *Angew. Chem., Int. Ed.* **2014**, *53*, 5998−6001.

(34) The detailed temperature dependences of the various transformations here and below are being investigated and will be published separately.

(35) Muan, A. On the Stability of The Phase Fe_2O_3-Al_2O_3. *Am. J. Sci.* **1958**, *256*, 413−422.

(36) Ketteler, G.; Weiss, W.; Ranke, W.; Schlögl, R. Bulk and Surface Phases of Iron Oxides in an Oxygen and Water. *Phys. Chem. Chem. Phys.* **2001**, *3*, 1114−1122.

(37) Ma, E.; He, J.-H.; Schilling, P. J. Mechanical alloying of immiscible elements: Ag-Fe contrasted with Cu-Fe. *Phys. Rev. B* **1997**, *55*, 5542−5545.

(38) Okamoto, H. Fe-Pt (Iron-Platinum). In *Phase Diagrams of Binary Iron Alloys*; Okamoto, H., Ed.; ASM International: Materials Park, OH, 1993; pp 330−336.

(39) Liu, Y.; Wang, J.; Du, Y.; Zhang, L.; Liang, D. Mobilities and diffusivities in fcc Fe−X (Ag, Au, Cu, Pd and Pt) alloys. *CALPHAD* **2010**, *34*, 253−262.

(40) Morrall, P.; Schedin, F.; Case, G. S.; Thomas, M. F.; Dudzik, E.; van der Laan, G.; Thornton, G. Stoichiometry of $Fe_{3-\delta}O_4$(111) Ultrathin Films on Pt(111). *Phys. Rev. B* **2003**, *67*, 214408−1 - 214408−7.

(41) Kachi, S.; Momiyama, K.; Shimizu, S. An Electron Diffraction Study and a Theory of the Transformation from γ-Fe_2O_3 to α-Fe_2O_3. *J. Phys. Soc. Jpn.* **1963**, *18*, 106−116.

(42) Carter, C. B.; Schmalzried, H. The Growth of Spinel into Al_2O_3. *Philos. Mag. A* **1985**, *52*, 207−224.

(43) Schmalzried, H. *Chemical Kinetics of Solids*; Wiley-VCH: Weinheim, Germany, 2008.

(44) Hesse, D. The Submicroscopic Structure of Reaction Fronts in Solid-Solid Reactions and its Correlation with Reaction Mechanism and Kinetics. *Solid State Ionics* **1997**, *95*, 1−15.

(45) Peterson, N. L.; Chen, W. K.; Wolf, D. Correlation And Isotope Effects For Cation Diffusion In Magnetite. *J. Phys. Chem. Solids* **1980**, *41*, 709−719.

(46) Lewis, G. V.; Catlow, C. R. A.; Cormack, A. N. Defect Structure And Migration In Fe_3O_4. *J. Phys. Chem. Solids* **1985**, *46*, 1227−1233.

(47) Nie, S.; Starodub, E.; Monti, M.; Siegel, D. A.; Vergara, L.; El Gabaly, F.; Bartelt, N. C.; de la Figuera, J.; McCarty, K. F. Insight into Magnetite's Redox Catalysis from Observing Surface Morphology during Oxidation. *J. Am. Chem. Soc.* **2013**, *135*, 10091−10098.

(48) Atkinson, A.; Taylor, R. I. Diffusion Of ^{55}Fe In Fe_2O_3 Single Crystals. *J. Phys. Chem. Solids* **1985**, *46*, 469−475.